Assessment of Alternative Methods for Analyzing X-ray Fluorescence Spectra

Michel N. Nader[1] and David E.B. Fleming[1]

[1]Physics Department, Mount Allison University, 67 York Street, Sackville, New Brunswick, Canada.

Corresponding author e-mail: dfleming@mta.ca

Abstract:

When analyzing characteristic peaks in X-ray fluorescence (XRF) spectra, the peak area is the value most often used to quantify peak size. However, some studies have reported the amplitude of the peak instead of the area. When the width of the peak is allowed to vary from trial to trial in order to provide the best possible fit to the data, these two alternative methods can yield slightly different results. In the current study, these two approaches to peak analysis are compared for data obtained from bone reference materials having certified lead concentrations of 1.09 ± 0.03 μg/g, 16.1 ± 0.3 μg/g, 13.2 ± 0.3 μg/g, and 31.5 ± 0.7 μg/g. Measurements were made with an Olympus Innov-X Delta Premium portable XRF system. Using both the area and amplitude methods, lines of best fit were constructed for the lead Lα and lead Lβ signals as a function of lead concentration. Additionally, coefficients of variation were calculated for each reference material and condition of analysis. To assess possible variations over time, the procedure was performed at two points separated by about one year. The amplitude and area methods were found to produce results which were consistent and proportional. Using either method, lead XRF signal plotted as a function of known lead concentration produced adjusted r^2 values of ~0.99. The amplitude method provided slightly higher adjusted r^2 values overall. Coefficients of variation were generally very similar between the two methods, although more pronounced differences emerged from measurements of the lowest concentration reference material.

Keywords: x-ray fluorescence; spectral analysis

Introduction:

X-ray fluorescence (XRF) is a non-destructive, convenient, and fast technique which may be used to assess the elemental composition of a sample. By bombarding the sample with X-rays or γ-rays having energy greater than the binding energy of the electrons of a particular element or elements, electrons may be ejected via the photoelectric effect. Within a given atom, an electron from a higher energy orbital may then replace an ejected electron. Such an electron transition can then be accompanied by the release of a characteristic X-ray, having an energy corresponding to the nature of the transition and the element. Characteristic X-rays recorded by a radiation detector thus provide information on the composition of the sample. The number of detected counts, plotted as a function of energy, produces an XRF spectrum with characteristic energy peaks corresponding to the various elements within the sample. Analysis of these peaks can help determine the concentration of the elements in the sample.

An XRF spectrum has two main components to consider: the continuum (or background noise), and the characteristic X-ray peaks. The continuum is a base level of counts, and may increase or decrease as a function of energy over a certain region of the spectrum. The continuum is caused primarily by scattered photons reaching the detector, and its contribution may be well approximated by a linear function over some regions of the spectrum or an exponential function over other regions. The characteristic X-ray peak from a particular element of interest is a signal located on top of the continuum. A Gaussian function is used to model a given signal peak:

$$f(x) = he^{\frac{-(x-\mu)^2}{2\sigma^2}} \quad \text{or} \quad f(x) = \frac{A}{\sigma\sqrt{2\pi}} e^{\frac{-(x-\mu)^2}{2\sigma^2}}$$

where h is the height (or amplitude) of the Gaussian function, μ is the center of the function, σ is the standard deviation of the function, and A is the area of the peak. [1] The standard deviation of

the Gaussian function also relates directly to the peak's full width at half of the maximum height, or the full width half max (FWHM), through the approximate relationship: $FWHM = 2.35\sigma$ (Knoll, 2000). Figure 1 illustrates these parameters using an actual XRF spectrum peak, fitted by a Gaussian function on top of the continuum (background).

For a fixed measurement condition and type of sample, the size of the characteristic peak from a given element is proportional to the concentration of that element in the sample. When fitting the data using a Gaussian function, the size of a given peak can be quantified in two different ways, using either the peak amplitude or the area of the peak (Van Grieken and Markowicz, 1993). The area of the peak is normally preferred since, in principle, it is expected to result in a lower statistical uncertainty (Van Grieken and Markowicz, 1993). Indeed, the primary literature on the use of XRF spectroscopy for measuring samples generally reflects adoption of the area method of analysis (Moise et al., 2014; Da Silva et al., 2013; Moise et al., 2012; Zamburlini et al., 2007; Desouza et al., 2013; Luo et al., 2007). However, from experience working with both methods, our group has favored the amplitude approach (Fleming and Ware, 2017; Fleming et al., 2017; Gherase et al., 2017; Groskopf et al., 2017; McIver et al., 2015; Fleming et al., 2015a; Fleming et al., 2015b). We have not, to this point, provided justification for this preference. Certainly, when the amplitude method has been used in the assessment of standard addition calibration phantoms, plots of amplitude against known phantom concentration have been highly linear. In recent studies, coefficients of determination (r^2) for such lines of calibration have reached or exceeded 0.99 (Fleming and Ware, 2017; Fleming et al., 2017). These results in themselves, however, are not sufficient justification for preferring the amplitude approach over the area approach. It may be important for future measurement applications involving medical samples to more closely

examine these two alternative approaches to the analysis of XRF spectra. The purpose of the current study is therefore to directly compare results, obtained under carefully controlled experimental conditions using certified reference materials, from both the peak area and the peak amplitude methods.

Materials and Method:

To provide an effective and valuable comparison of the peak area and peak amplitude methods of data analysis requires a very particular type of sample set. An ideal sample set would consist of a variety of individual samples with well-defined concentrations of a particular element. In addition, the samples within the set should span a range of concentrations, be uniform in size and shape, homogeneous in composition, and model a biologically relevant measurement. For these reasons, we selected as our sample set a group of bone reference materials, produced from a population of goats (caprines) and cows (bovines) maintained by the New York State Department of Health (NYSDOH) (Bellis et al., 2008).

As described previously (Bellis et al., 2008), for the purpose of evaluating analytical methods for lead detection and measurement, the NYSDOH maintained a herd of goats and cows which were regularly dosed with known amounts of lead acetate according to a standard protocol. The protocol (01-096) was approved by the NYSDOH Wadsworth Center Institutional Animal Care and Use Committee. The tibia, femur, humerus, and radius bones were harvested from the goats and cows *post mortem*, stripped of adhered tissue, and cleaned of remaining tissue using hydrogen peroxide and ether (Bellis et al., 2008). The bones were pooled into four different levels of lead dosage, shattered, ground, homogenized, and vacuum-sealed with a thin layer of

plastic into disks labeled 05-01 through 05-04, with each disk presenting a different concentration of lead (Bellis et al., 2008). Each disk had the same size, with a diameter of 4.0 cm and a thickness of 0.8 cm. The complete set of reference materials thus produced consists of four disks having lead concentrations of 1.09 ± 0.03 μg/g (05-01), 16.1 ± 0.3 μg/g (05-02), 13.2 ± 0.3 μg/g (05-03), and 31.5 ± 0.7 μg/g (05-04) (Bellis et al., 2008). The concentrations of these disks were determined to high precision using isotope dilution inductively coupled plasma mass spectrometry (ID-ICP-MS), and confirmed through inter-laboratory comparisons using a variety of methods including ICP-MS and electrothermal atomic absorption spectrometry (ETAAS) (Bellis et al., 2008).

For the purpose of this study, the disks were analyzed using a portable XRF Olympus Innov-X Delta Premium (DP-2000) system in tabletop mode (Figure 2) (Innov-X Technologies Canada; Vancouver, BC). The system used a peak voltage of 40 kV and a beam current of 37 μA. Each of the four disks was initially measured in 2016 for 180 seconds (real time) per trial for five trials, resulting in 20 energy spectra. The entire measurement procedure was repeated approximately one year following the initial measurements, resulting in an additional 20 energy spectra. The purpose of this additional set of measurements was to investigate whether variations in overall results may be expected to occur as a function of time or measurement condition.

During data analysis, the uncertainty associated with the count in each energy channel was determined (see, for example, Figure 1). The energy range of interest was 10 keV to 13 keV, encompassing the Pb Lα and Lβ peaks at 10.5 keV and 12.6 keV, respectively (Kortright and Thompson, 2001). As a consequence of the X-ray detector and the plastic packaging of the disks,

two additional peaks were also present in the spectra: a Au Lβ peak at 11.5 keV and a Br Kα peak at 11.9 keV (Kortright and Thompson, 2001). Each of the energy spectra was therefore fitted using a multi-parameter non-linear function, consisting of a series of Gaussian peaks on top of an exponential background. The software used to perform this fitting was OriginPro 9.1 (OriginLab Co., Northampton, MA). The complete fitting function had the following form:

$$f(x) = P1e^{-P2(x-P3)^2} + P4e^{-P5(x-P6)^2} + P7e^{-P8(x-P9)^2} + P10e^{-P11(x-P12)^2} + P13e^{P14x} + P15$$

Here, the P1, P4, P7, and P10 parameters were the amplitudes (h) of the Pb Lα, Au Lβ, Br Kα, and Pb Lβ Gaussian peaks, respectively. Likewise, the P2, P5, P8, and P11 parameters represented half of the inverse square of the standard deviation $\left(\frac{1}{2\sigma^2}\right)$ of the same four peaks. The P3, P6, P9, and P12 parameters were the energies (μ) at which the peaks for Pb Lα, Au Lβ, Br Kα, and Pb Lβ were centered. To achieve the best functional fit to the data, the μ values were allowed to vary ±0.1 keV from their initial input values of 10.5 keV (for Pb Lα), 11.5 keV (for Au Lβ), 11.9 keV (for Br Kα), and 12.6 keV (for Pb Lβ). Likewise, the $\left(\frac{1}{2\sigma^2}\right)$ values were permitted to vary over a small range. Finally, the P13, P14, and P15 parameters modeled the shape of the continuum or background. The Origin software provided a best fit output value for each of these parameters, with a corresponding standard error.

It should be noted that the four Gaussian peaks described above each individually included detections of multiple characteristic X-ray contributions having slightly *different* transition energies. For example, the Pb Lα peak included contributions from $L\alpha_1$ (10.55 keV) and $L\alpha_2$ (10.45 keV). Nonetheless, the use of a single peak to fit this type of data has been common when the separation between the different energies is small relative to the energy resolution of the

detector (Zamburlini et al., 2007; Luo et al., 2007; Moise et al., 2014). From the output values for the parameters mentioned above it was then straightforward to arrive at the two desired measures of size for a given peak: the amplitude of the peak and the area of the peak. The amplitude in each case was provided directly from the fitting output, as described above. The area was calculated from the amplitude and width of the peak, according to the following equation:

$$A = \frac{h}{0.3989}\sigma$$

Here, A represents the area of the peak, h is again the amplitude of the peak, and σ is the standard deviation of the peak (Gaussian function). It is important to note that, were the σ value held fixed from trial to trial, the A result and the h result would differ only by a constant. However, in this study, the σ value was allowed to vary from trial to trial in order to provide the best possible fit to the data.

For each of the measurement trials performed we thus determined the amplitude and area for each peak. In this study, the Pb Lα and Pb Lβ peaks were the two peaks of interest, since they were expected to directly reflect the concentration of lead within the various reference materials. The mean and sample standard deviation from both the amplitude results and the area results were determined for the Pb Lα and Pb Lβ peaks from both 2017 and 2016, using each of the reference materials in turn (05-01, 05-02, 05-03, and 05-04). These results were plotted as a function of the known lead concentrations from the reference materials. Lines of best fit were determined for the results as a function of lead concentration. Correlations between the amplitude results and the lead concentrations, and between the area results and the lead

concentrations, were examined. The adjusted r^2 values (coefficients of determination) from the lines of best fit were used to compare between the amplitude and area methods. In addition, the reproducibility of measurement from each group of five trials, using both the peak amplitude and area methods, were compared using the coefficient of variation (CV):

$$CV = \left(1 + \frac{1}{4n}\right)\frac{s}{\bar{x}} \times 100\%$$

Here, $\bar{x}$ is the mean result, s is the sample standard deviation, and n is the number of trials. It was anticipated that the coefficient of variation would be informative when comparing the consistency of results obtained from the amplitude and area methods, in particular for the lowest lead concentration reference material (05-01).

Results:

Two typical energy spectra, and their associated functional fits, are provided in Figure 3. These two spectra represent measurements from: a) the reference material having the highest lead concentration (05-04); and b) the reference material having the lowest lead concentration (05-01). The four peaks of interest over the energy range shown are those from Pb Lα (10.5 keV), Au Lβ (11.5 keV), Br Kα (11.9 keV), and Pb Lβ (12.6 keV). The functional fits were successful in fitting the data for all of the different trials performed. The average reduced χ^2 results ranged from 1.02 (for reference material 05-02) to 1.17 (05-01) for the 2017 measurements, and from 1.01 (05-04) to 1.12 (05-02) for the 2016 measurements. It is clear from Figure 3 that the Pb Lα and Pb Lβ peaks vary in size with lead concentration. For all measurements performed (both in 2017 and 2016), the size of these peaks was assessed using both the amplitude and area methods. In each case, the average results from five trials and the standard deviation of these results are shown, as a function of the reference material lead concentration, in Figures 4 and 5. Figure 4a

provides the lines of best fit for the Pb Lα peak assessed from the 2017 trials, Figure 4b for the Pb Lβ peak from the 2017 trials, Figure 5a for the Pb Lα peak from the 2016 trials, and Figure 5b for the Pb Lβ peak from the 2016 trials. Table 1 summarizes these same results in terms of parameters from the lines of best fit, including the adjusted r^2 values. Coefficients of variation from the five trials under each experimental condition, and using both the amplitude and area methods, were also reviewed. Coefficients of variation from the two methods are presented as a function of reference material lead concentration in Figures 6 and 7.

Discussion:

The data presented above highlight broad similarities and subtle differences in the results obtained between the amplitude and area methods of analysis. Overall, the amplitude and area methods return results which are proportional to each other in a consistent way, and that increase in a linear fashion as a function of lead concentration. This is clearly illustrated by Figures 4 and 5. The generally consistent proportionality of results holds regardless of whether one examines the alpha peak results, the beta peak results, the results from 2016, or the results from 2017. The slopes and intercepts of the lines of best fit in Table 1 highlight the consistency of results from both methods of analysis between 2016 and 2017. As shown by the adjusted r^2 results in Table 1, typically greater than 99% of the observed variance in the amplitude (or the area) of a peak is accounted for by the lead concentration. The only deviation from this general trend came from a slightly lower adjusted r^2 result (0.983) when using the area analysis method with the 2017 Lβ fits. Notably, the adjusted r^2 value is slightly higher when using the amplitude method as opposed to the area method for all four head-to-head comparisons from Table 1 (2017 Lα, 2017 Lβ, 2016 Lα, 2016 Lβ).

Examining the coefficient of variation outcomes, the amplitude and area methods produced results which were generally very similar to each other for the trials involving the reference materials 05-02, 05-03, and 05-04. The one exception to this was from the 2016 Pb Lβ measurements of the reference material 05-02, where the amplitude method returned a lower coefficient of variation (Figure 7). However, for reference material 05-01 (having the relatively low lead concentration of 1.09 ± 0.03 μg/g), more pronounced differences between the two methods were evident. The amplitude method resulted in a consistently smaller coefficient of variation for the Lα peak (2016 and 2017 data) and a slightly lower coefficient of variation for the 2016 Pb Lβ peak, but a higher coefficient of variation for the 2017 Lβ peak (Figures 6 and 7). Notably, the peak widths (or Gaussian σ values) were generally very similar between the Pb Lα and Pb Lβ detection peaks. Excluding reference material 05-01 (for which the peaks were difficult to fit consistently), the average peak widths agreed within 5% between the Pb Lα and Pb Lβ fits for both the 2016 and 2017 data.

Overall, one apparent conclusion from this study is that there is little difference resulting from analysis using the amplitude method and analysis using the area method. This is not at all surprising given the very similar underlying nature of the two methods. As noted above, if a constant peak width (or Gaussian σ value) were assigned and maintained, the two methods would essentially reduce to being equivalent. Where there are any differences observed between the two methods, they emerge from slight trial to trial variations in the fitting of peak widths to the data. The results here suggest that such differences are most likely to arise when analyzing low concentration samples. This makes sense since the signal resulting from a low concentration sample is inherently more difficult to fit, and therefore more susceptible to random fluctuations

in the data. It appears that variations in results from the amplitude method are less pronounced than variations in results from the area method, suggesting slightly more robust results when using the amplitude method. From the current data, however, there is little to suggest a strong preference between the amplitude method and the area method of analysis. The amplitude method does present a slightly higher degree of linearity in plots of signal against known concentration (Table 1), and a slight tendency for smaller coefficients of variation between trials (Figures 6 and 7). These findings are consistent with previous experience, which has led our group to favor the amplitude method in the past (Fleming and Ware, 2017; Fleming et al., 2017; Gherase et al., 2017; Groskopf et al., 2017; McIver et al., 2015; Fleming et al., 2015a; Fleming et al., 2015b).

Beyond a comparison of the amplitude and area methods of analysis, other points of interest also emerge from the current results. For example, examining the *ratio* of the slope results obtained between the amplitude and area methods as a function of lead concentration is informative. From Table 1, the ratio of the amplitude slope to the area slope provides results of 4.80 ± 0.14 from the 2017 Lα measurements, 4.71 ± 0.43 from the 2017 Lβ measurements, 4.88 ± 0.17 from the 2016 Lα measurements, and 4.82 ± 0.18 from the 2016 Lβ measurements. Although all four of these ratios are consistent with each other within uncertainty, two trends are suggested: (1) the Lα ratios are slightly greater than the Lβ ratios for a given year; and (2) the 2016 ratios are slightly greater than the 2017 ratios for a given characteristic X-ray. Both of these trends reflect expected results in the following sense: if we consider two of the relationships provided above, $A = \frac{h}{0.3989}\sigma$ and FWHM = 2.35σ, the ratio of amplitude (h) to area (A) can be mathematically related to the FWHM of the Gaussian peak. This ratio is inversely related to FWHM, such that a higher

ratio implies a smaller FWHM. (It should be noted that this analysis assumes a constant value of σ for a given characteristic X-ray peak and year of measurement. As mentioned previously, this assumption does not always hold, but in a general sense σ was very nearly constant for such trials.) Given this inverse relationship between the ratio and FWHM, our ratio results indicate slightly smaller FWHMs from the Lα measurements (relative to Lβ) and from the 2016 measurements (relative to 2017). In the case of the Lα measurements, this is expected since Lα X-rays (10.5 keV) are detected at a lower energy than Lβ X-rays (12.6 keV), and the FWHM should increase with energy due to statistical considerations (Knoll, 2000). Likewise, when comparing the 2016 and 2017 measurements, the FWHM is expected to gradually increase for a given detector over time due to gradual physical degradation of the system (Shanmugam et al., 2015).

In summary, the current study provided a series of results from analyses of XRF spectra, obtained from the measurement of bone reference materials having known concentrations of lead. Two distinct but related methods of quantifying the size of the lead peaks were considered: one method used the peak area, while the other method used the peak amplitude. The results of the study were largely consistent with expectation and well established understanding of XRF spectral analysis. The results, however, also suggested that the amplitude method of peak analysis is a valid alternative to the more conventionally employed area method.

Acknowledgements:

This work was supported by a Discovery Grant from the Natural Sciences and Engineering Research Council of Canada.

References:

Bellis, D.J., Hetter, K.M., Verostek, M.F., Parsons, P.J. (2008). Characterization of candidate reference materials for bone lead via interlaboratory study and double isotope dilution mass spectrometry. *Journal of Analytical Atomic Spectrometry*, 23: 298-308.

Da Silva, E., Kirkham, B., Heyd, D.V., Pejović-Milić, A. (2013). Pure hydroxyapatite phantoms for the calibration of in vivo X-ray fluorescence systems of bone lead and strontium quantification. *Analytical Chemistry*, 85: 9189-9195.

Desouza, E.D., Atiya, I.A., Al-Ebraheem, A., Wainman, B.C., Fleming, D.E., McNeill, F.E., Farquharson, M.J. (2013). Characterization of the depth distribution of Ca, Fe and Zn in skin sample, using synchrotron micro-x-ray fluorescence (SμXRF) to help quantify in-vivo measurements of elements in the skin. *Applied Radiation and Isotopes,* 77: 68-75.

Fleming, D.E.B., Foran, K.A., Kim, J.S., Guernsey, J.R. (2015). Portable x-ray fluorescence for assessing trace elements in rice and rice products: Comparison with inductively coupled plasma-mass spectrometry. *Applied Radiation and Isotopes,* 104: 217-223.

Fleming, D.E.B., Groves, J.W., Gherase, M.R., George, G.N., Pickering, I.J., Ponomarenko, O., Langan, G., Spallholz, J.E., Alauddin, M., Ahsan, H., Ahmed, S., La Porte, P.F. (2015). Soft tissue measurement of arsenic and selenium in an animal model using portable x-ray fluorescence. *Radiation Physics and Chemistry,* 116: 241-247.

Fleming, D.E.B., Nader, M.N., Foran, K.A., Groskopf, C., Reno, M.C., Ware, C.S., Tehrani, M., Guimarães, D., Parsons, P.J. (2017). Assessing arsenic and selenium in a single nail clipping using portable X-ray fluorescence. *Applied Radiation and Isotopes,* 120: 1-6.

Fleming, D.E.B., Ware, C.S. (2017). Portable x-ray fluorescence for the analysis of chromium in nail and nail clippings. *Applied Radiation and Isotopes*, 121: 91-95.

Gherase, M.R., Feng, R., Fleming, D.E.B. (2017). Optimization of L-shell x-ray fluorescence detection of lead in bone phantoms using synchrotron radiation. *X-Ray Spectrometry,* 46: 537-547.

Groskopf, C., Bennett, S.R., Gherase, M.R., Fleming, D.E.B. (2017). Detection of lead in bone phantoms and arsenic in soft tissue phantoms using synchrotron radiation and a portable x-ray fluorescence system. *Physiological Measurement,* 38: 374-386.

Knoll, G.F., 2000. Radiation Detection and Measurement, third ed. John Wiley & Sons, Inc., New York.

Kortright, J.B., Thompson, A.C., 2001. X-Ray emission energies, in: Thompson, A.C., Attwood, D.T., Gullikson, E.M., Howells, M.R., Kim, K.-J., Kirz, J., Kortright, J.B., Lindau, I., Pianetta, P., Robinson, A.L., Scofield, J.H., Underwood, J.H., Vaughan, D., Williams, G.P., Winick, H.

(Eds.), X-Ray Data Booklet, second ed. Lawrence Berkeley National Laboratory, Berkeley, pp. 1-15 – 1-27.

Luo, L., Chettle, D.R., Nie, H., McNeill, F.E., Popovic, M. (2007). The effect of filters and collimators on Compton scatter and Pb K-series peaks in XRF bone lead analysis. *Nuclear Instruments and Methods in Physics Research B*, 263: 258-261.

McIver, D.J., VanLeeuwen, J.A., Knafla, A.L, Campbell, J.A., Alexander, K.M., Gherase, M.R., Guernsey, J.R., Fleming, D.E.B. (2015). Evaluation of a novel portable x-ray fluorescence screening tool for detection of arsenic exposure. *Physiological Measurement*, 36: 2443-2459.

Moise, H., Adachi, J.D., Chettle, D.R., Pejović-Milić, A. (2012). Monitoring bone strontium levels of an osteoporotic subject due to self-administration of strontium citrate with a novel diagnostic tool, in vivo XRF: A case study. *Bone,* 51: 93-97.

Moise, H., Chettle, D.R., Pejović-Milić, A. (2014). Monitoring bone strontium intake in osteoporotic females self-supplementing with strontium citrate with a novel in-vivo X-ray fluorescence based diagnostic tool. *Bone*, 61: 48-54.

Shanmugam, M., Acharya, Y.B., Vadawale, S.V., Mazumdar, H.S. (2015). Radiation effects on Silicon Drift Detector based X-ray spectrometer on-board Chandrayaan-2 mission. *Journal of Instrumentation,* 10: P09005.

Van Grieken, R.E., Markowicz, A.A. (Eds.), 1993. Handbook of X-Ray Spectrometry: Methods and Techniques. Marcel Dekker, Inc., New York.

Zamburlini, M., Pejović-Milić, A., Chettle, D.R., Webber, C.E., Gyorffy, J. (2007). In vivo study of an x-ray fluorescence system to detect bone strontium non-invasively. *Physics in Medicine and Biology,* 52: 2107-2122.

Figures

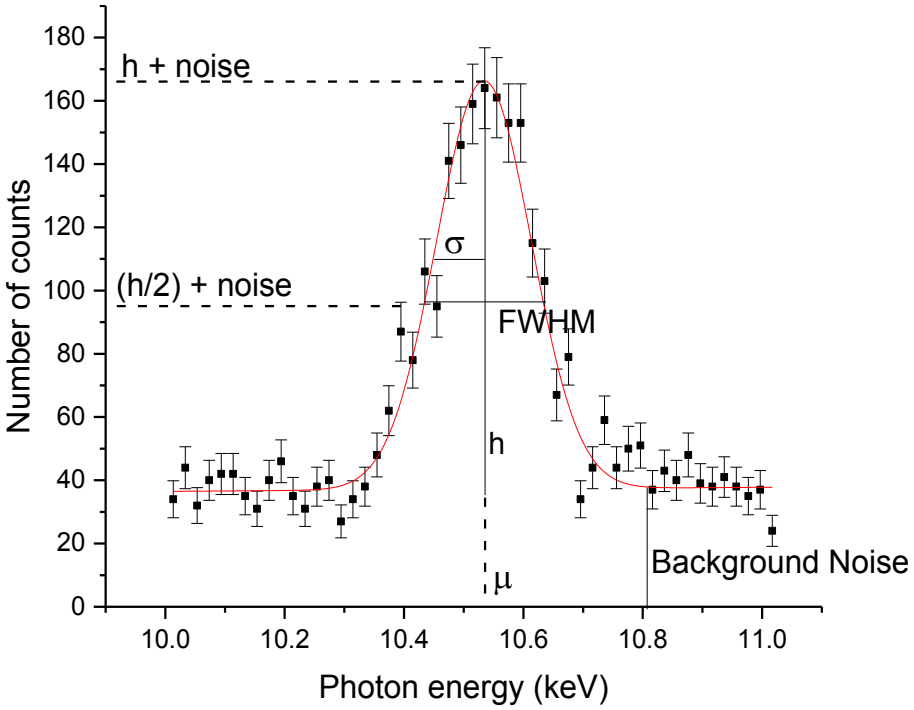

Figure 1: XRF spectrum peak fitted using a Gaussian function. The standard deviation, full width half max, peak amplitude, and peak center are labeled here as σ, FWHM, h, and μ, respectively.

Figure 2: The portable XRF Olympus Innov-X Delta Premium DP-2000 system setup in tabletop mode.

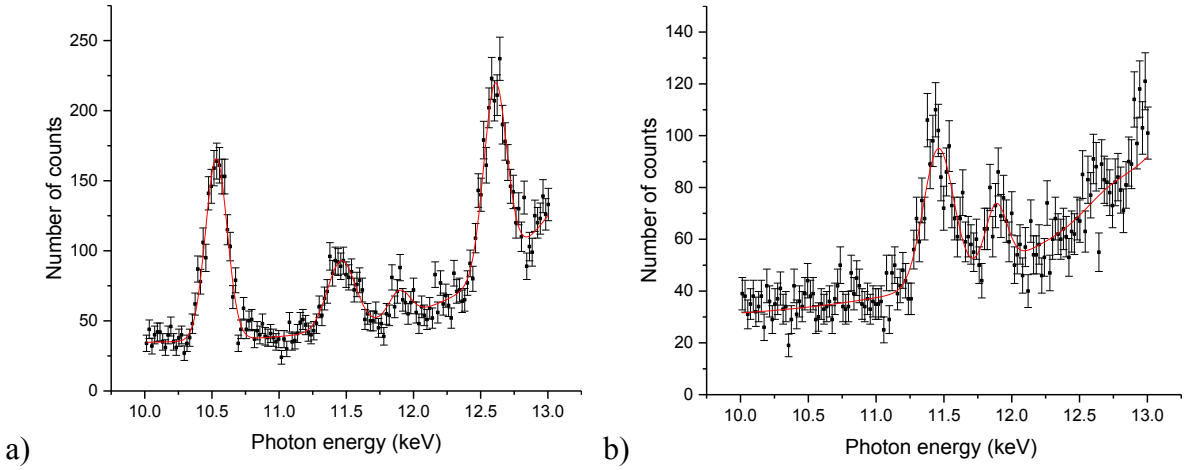

Figure 3: XRF spectra from the first measurement trials performed with reference materials a) 05-04 and b) 05-01 in 2017. The spectra are fit using a non-linear function consisting of Gaussian peaks on top of the continuum.

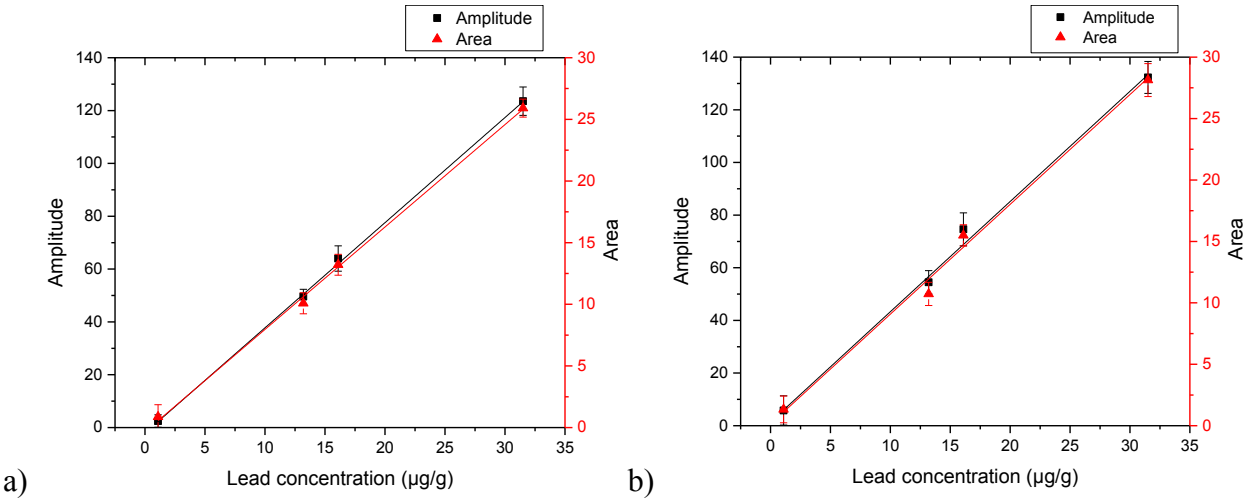

Figure 4: a) Lines of best fit from the amplitude and area average results for the Pb Lα peak from trials performed in 2017. b) Lines of best fit from the amplitude and area average results for the Pb Lβ peak from trials performed in 2017.

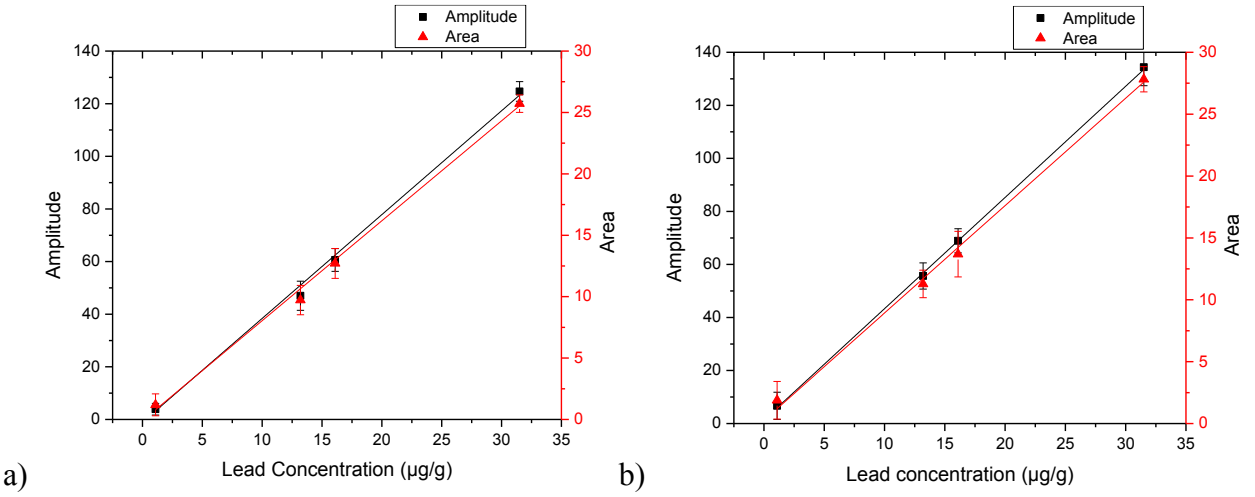

Figure 5: a) Lines of best fit from the amplitude and area average results for the Pb Lα peak from trials performed in 2016. b) Lines of best fit from the amplitude and area average results for the Pb Lβ peak from trials performed in 2016.

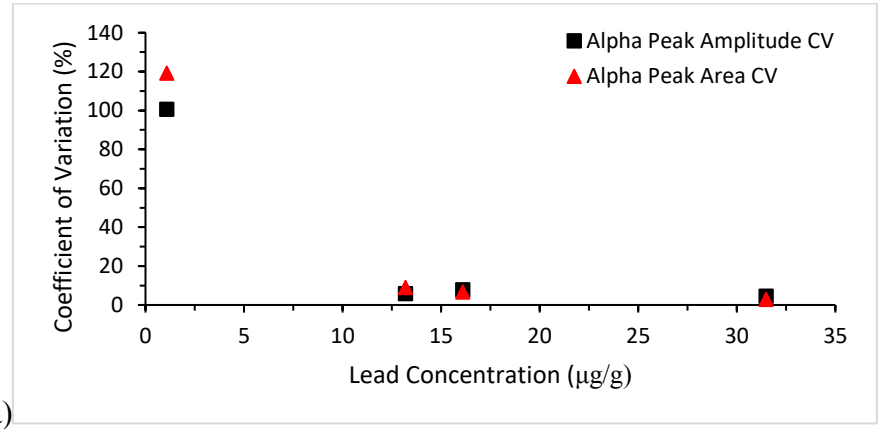

a)

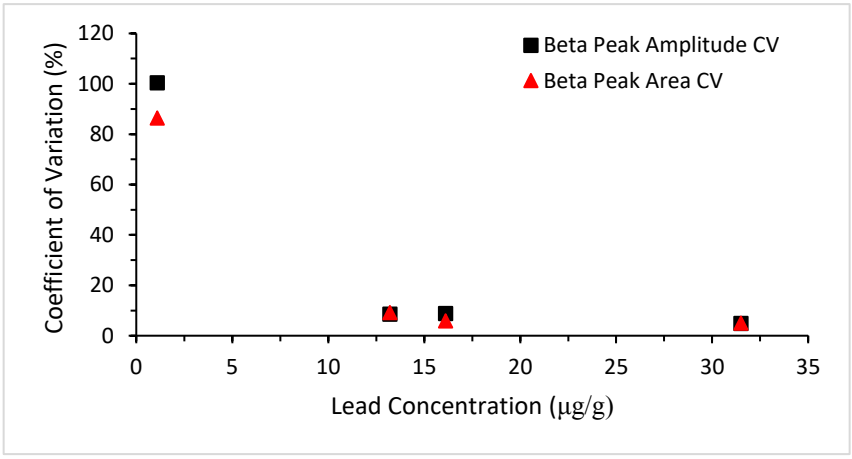

b)

Figure 6: a) Coefficient of variation associated with the amplitude and area results for the Pb Lα peak from measurements performed in 2017. b) Coefficient of variation associated with the amplitude and area results for the Pb Lβ peak from measurements performed in 2017.

a)

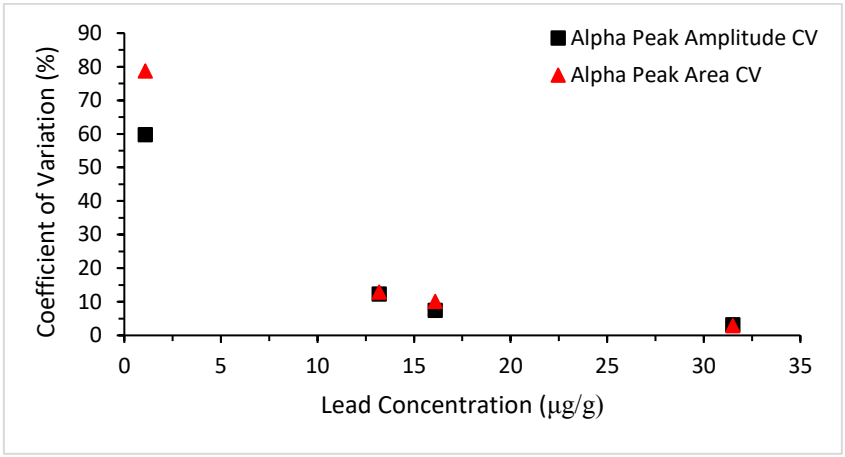

b)

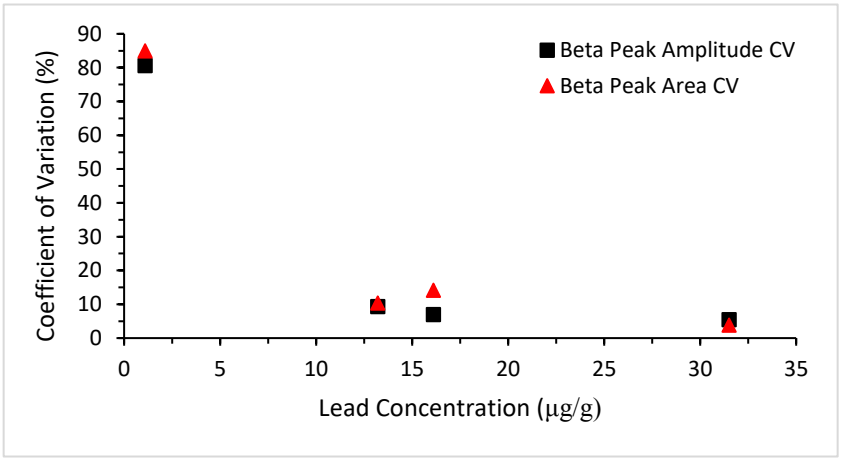

Figure 7: a) Coefficient of variation associated with the amplitude and area results for the Pb Lα peak from measurements performed in 2016. b) Coefficient of variation associated with the amplitude and area results for the Pb Lβ peak from measurements performed in 2016.

Tables

Table 1: Adjusted r^2, slope, and y-intercept of the lines of best fit for the amplitude and area as a function of lead concentration. Results are presented from the analysis of the Lα and Lβ peaks, for measurements made in 2017 and 2016.

Year of measure	Pb peak	Analysis method	Adjusted r^2	Slope	Slope uncertainty	y-intercept	y-intercept uncertainty
2017	Lα	Amplitude	0.99921	3.98	0.065	-2.03	0.86
		Area	0.99822	0.83	0.02	-0.34	0.42
	Lβ	Amplitude	0.99304	4.19	0.20	1.44	3.57
		Area	0.98273	0.89	0.07	0.15	1.15
2016	Lα	Amplitude	0.99824	3.95	0.10	-1.04	1.52
		Area	0.99718	0.81	0.02	-0.09	0.55
	Lβ	Amplitude	0.99943	4.19	0.06	1.41	0.95
		Area	0.99696	0.87	0.03	0.26	0.60